1-1-2016

Induction Local Softening Of Advanced High Strength Steel

Jorge Saul Cisneros
Wayne State University, jscisneros@gmail.com

Recommended Citation

Cisneros, Jorge Saul, "Induction Local Softening Of Advanced High Strength Steel" (2016). *Wayne State University Theses*. 698.
https://digitalcommons.wayne.edu/oa_theses/698

INDUCTION LOCAL SOFTENING OF ADVANCED HIGH STRENGTH STEEL

by

JORGE CISNEROS

THESIS

Submitted to the Graduate School

of Wayne State University,

Detroit, Michigan

in partial fulfillment of the requirements

for the degree of

MASTER OF SCIENCE

2018

MAJOR: MECHANICAL ENGINEERING

Approved By:

2/5/2018

Xin Wu Date

ACKNOWLEDGEMENTS

Many thanks to my parents for their encouragement of continuing my education and helping to fund both classes and my research. Thank you to Dr. Xin Wu for his guidance, inspiration, equipment, and materials. The trip to Argonne National lab changed everything.

This study is supported by US Department of Energy-US Advanced Materials Partnership (DOE-USAMP) under Award Number DE-FC26-02OR22910 and subcontracted from Auto Steel Partnership (A/SP) under contract No. 440850, and by matching fund from member companies. The assistance by Dr. Yang Ren of Argonne National Laboratory on Synchrotron analysis is greatly appreciated.

TABLE OF CONTENTS

LIST OF TABLES

LIST OF FIGURES

CHAPTER 1: INTRODUCTION

1.1 Introduction and Motivation

Advanced high strength steels (AHSS) have become an important material used by the automotive industry today. Increasing demands for lighter safer vehicles has fueled their use. They are used where design requires high strength, good crashworthiness, and good formability, such as wheel, bumper and other body structures. The AHSS are also cost competitive with traditional carbon steels. Despite the many promising properties, AHSS have a few technical problems to solve when used in manufacturing.

The microstructure of the AHSS plays a crucial role in the performance and behavior of the material. They are typically in multiple phases, which contain martensite, bainite, and/or retained austenite. Many types of AHSS exist, these include dual-phase (DP) steels, transformation induced plasticity (TRIP) steels, martensitic (MS) steels, complex phase (CP) steels, hot forming (HF) steels, and twinning-induced plasticity (TWIP) steels. Of these DP and TRIP steels are extensively used in sheet forming of automotive parts. These steels are characterized by higher yield strength, lower ductility, limited formability, and show low post necking deformation. As a result, there are some challenges which need to be addressed with conventional forming of AHSS.

One possible solution for better forming is local softening through heating. The heating can be achieved in a variety of ways, such as furnace heating, electrical resistive heating, and induction heating. The automotive industry requires fast reliable manufacturing methods, which makes induction heating the most practical choice. Induction heating has been shown to have the fastest heating time with good control over heat affected zone. However, this leads to a wide range of possible effects to the material, as a result studies will need to be conducted to fully understand how the AHSS change.

The current techniques for analyzing the effects of induction softening can be quite time consuming. It is difficult to obtain optical microstructure images, which provide accurate results, due to the fine grain of the microstructure. It is also a challenging task to prepare samples and obtain accurate analysis from technique such as scanning electron microscope, and orientation imaging microscope with electron backscatter diffraction. Therefore, effort was made to use newer techniques such as high energy X-ray diffraction. This allows for a fast and accurate method to determine the percentage of phase in the microstructure. It can also be used In-Situ to determine the phase changes during heating and the effect of holding time and cooling rate on the final phase. The effect of induction softening is the focus of this study. Before discussing the effect of softening, the scope and objective of this thesis is presented, followed by a survey of classes for AHSS and high energy X-ray diffraction are discussed.

1.2 Thesis Objective and Outline

The objective of this study on the effects of induction local softening of AHSS, is to identify what parameters can be used to tailor material properties for increased formability. The results of tensile tests, hardness tests, microstructure analysis, and high energy X-ray diffraction were used to generate a more complete understanding of the problem. The second objective of the study is to make recommendations for future studies.

Chapter 2 is a survey of various classes needed for background and understanding of AHSS, and prior research, Chapter 3 discusses the methods for conducting the experiments and analyzing the results, Chapter 4 presents and discusses the results of the experiments, and Chapter 5 is a summary of the results of this thesis work and future research.

CHAPTER 2: BACKGROUND AND PRIOR RESEARCH

2.1 Stress Strain and Plastic Strain Ratio r Definition

Stress and strain are produced when a material experiences a load with respect to a cross sectional area. The result is dependent on the loading direction with respect to microstructure orientation. A test apparatus provides data such as force and displacement, which can be processed to find the material properties and mechanical performance [1]. A variety of tests are performed to determine a material stress-strain behavior. These include uniaxial tensile test, uniaxial compression, biaxial tension, shear and/or planar tension. The uniaxial tensile test is the most common of these tests [2]. Stress and strain are calculated from measurements during a tensile test. The engineering stress S, and strain e, are calculated with Equations 2.1 and 2.2.

$$\boldsymbol{S} = \frac{\boldsymbol{F}}{\boldsymbol{A_0}} \tag{2.1}$$

And

$$\boldsymbol{e} = \frac{\Delta \boldsymbol{l}}{\boldsymbol{l_0}} \tag{2.2}$$

Where A_0 and l_0 are initial area and initial gauge length respectively, Δl is the change in length, and *F* is the Force. Initially the deformation is elastic, and the tensile force is linearly related to elongation, this is known as modulus of elasticity (E). Elastic deformation is recoverable. When the forced is increased beyond this point the material plastically deforms, this is referred to as yield stress(σ_y). Meaning it will not return to original shape if the load is released. Ductile materials stress reaches a maximum (UTS) then decrease until fracture. Figure 1 shows a typical engineering stress strain curve for a ductile material.

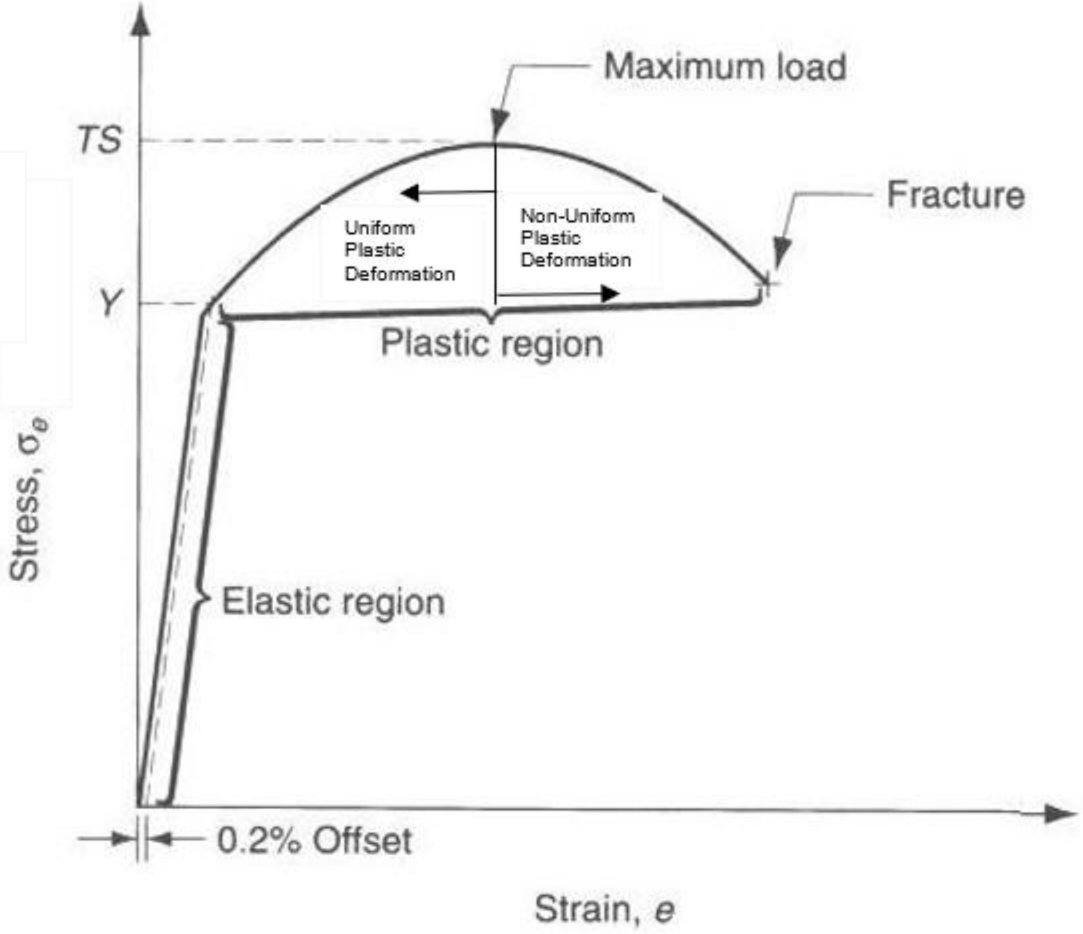

FIG. 1 Engineering Stress Strain Curve for Ductile Material

The engineering stress strain behavior is based on the original dimensions of the test specimen. However, the actual instantaneous area supporting the load becomes smaller as the load increases. Therefore, to find the true stress and strain Equations 2.3 and 2.4 are used.

$$\boldsymbol{\sigma = S * (1 + e)} \tag{2.3}$$

$$\boldsymbol{\varepsilon = \ln\left(\frac{l}{l_0}\right) = ln(1 + e)} \tag{2.4}$$

Here l is the instantaneous length. True strain is calculated from instantaneous change in length over the original length, when solved using calculus Equations 2.4 is derived. This is used to derive the instantaneous area and derive equation 2.3. True strains are actually consistent with a materials actual properties unlike engineering strain [1].

2.2 Review of AHSS

2.2.1 Need for AHSS

The increase in demand and requirements for lighter safer more fuel-efficient vehicles has led to an increase in the use of AHSS. Fuel efficiency is mainly controlled by the weight of the steel parts used in the vehicle, this is controlled by gauge and design. Safety is controlled by the energy absorbing characteristics of the steel. These are the two driving factor for auto makers increase use of AHSS to replace structural parts made with conventional steel in the past [3]. A study by J. Shaw and B. Zuidema showed sports wagons built from 1999-2005 used about 1% of AHSS, wagons built 2005-Present use about 7% AHSS [4]. Of the AHSS, DP and TRIP are the most extensively used in the manufacture of autobody parts.

2.2.2 Mechanical Properties of AHSS

The increased formability of AHSS is the main advantage over other conventional high strength steels. The ability of the material to undergo different forming modes without defects such as splitting, wrinkling is broadly termed as the "formability" of the material. However, AHSS has relatively low ductility compared to draw quality steel. AHSS enhanced characteristics are obtained from the microstructure. Table 1 is a brief summary of the metallurgy and general characteristic of AHSS [5]. In general, AHSS have similar carbon content as typical steel with a small addition of various elements as micro alloy, which helps control the final microstructure during annealing. The microstructure of AHSS is multiphase consisting of ferrite, martensite, austenite, and or bainite.

Table 1. Metallurgy and General Characteristics of Various Advanced High Strength Steel

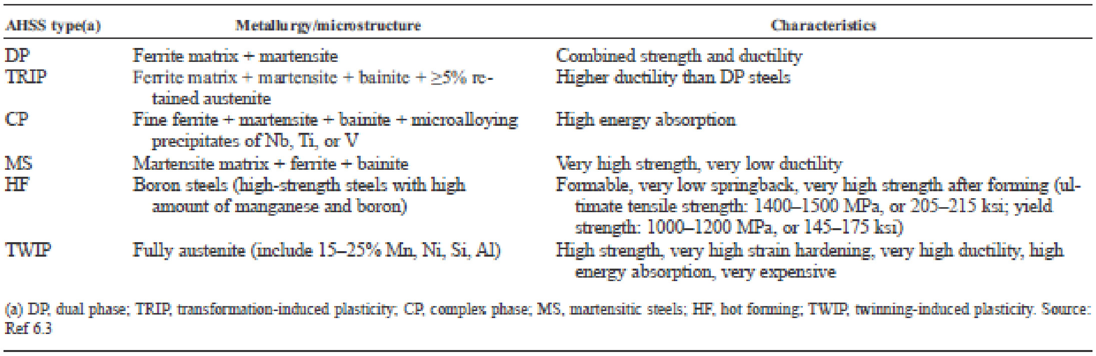

AHSS type(a)	Metallurgy/microstructure	Characteristics
DP	Ferrite matrix + martensite	Combined strength and ductility
TRIP	Ferrite matrix + martensite + bainite + ≥5% retained austenite	Higher ductility than DP steels
CP	Fine ferrite + martensite + bainite + microalloying precipitates of Nb, Ti, or V	High energy absorption
MS	Martensite matrix + ferrite + bainite	Very high strength, very low ductility
HF	Boron steels (high-strength steels with high amount of manganese and boron)	Formable, very low springback, very high strength after forming (ultimate tensile strength: 1400–1500 MPa, or 205–215 ksi; yield strength: 1000–1200 MPa, or 145–175 ksi)
TWIP	Fully austenite (include 15–25% Mn, Ni, Si, Al)	High strength, very high strain hardening, very high ductility, high energy absorption, very expensive

(a) DP, dual phase; TRIP, transformation-induced plasticity; CP, complex phase; MS, martensitic steels; HF, hot forming; TWIP, twinning-induced plasticity. Source: Ref 6.3

The microstructure plays an important role in the characteristics of the steel. Figure 2 shows the microstructure of DP steel, it is a matrix of light-colored ferrite with dark islands of martensite. During deformation the softer ferrite plastically deforms before the martensite [6]. There is a large stress concentration at the phase boundary of the ferrite during this process, which accounts for the high initial strain rate [7].

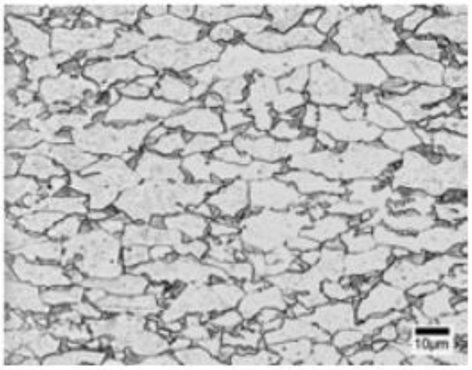

Fig 2. Typical Microstructure of DP Steel [3]

Figure 2 shows the relationship between total elongation and ultimate tensile strength for various AHSS. There is a large decrease in total elongation as the strength increase. The graph follows a banana shaped curve, with only Trip and DP steels tending towards higher ductility while having a higher tensile strength.

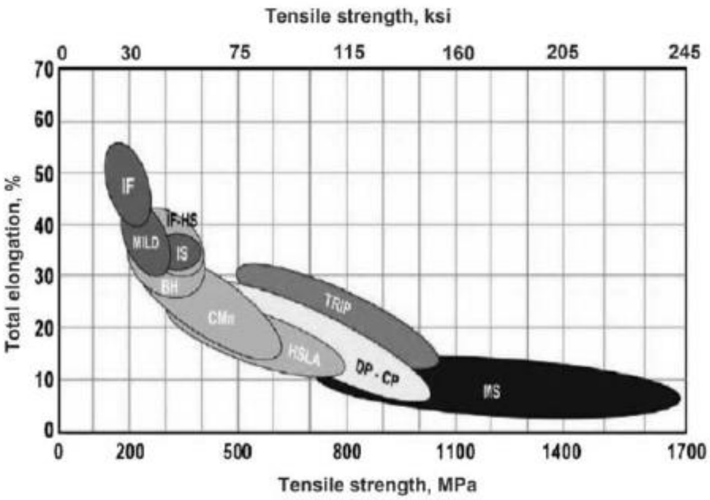

Fig 3. Total Elongation vs. Ultimate Tensile Strength [5]

The engineering stress strain curve for several DP steels and one TRIP are shown in Fig 3. The higher initial strain hardening of DP steels compared to TRIP steels is clear. The flow curves of AHSS around the UTS is almost flat as compared to conventional steel. IT can also be seen TRIP has a higher total elongation than other DP steels with the same UTS, this means it is more formable.

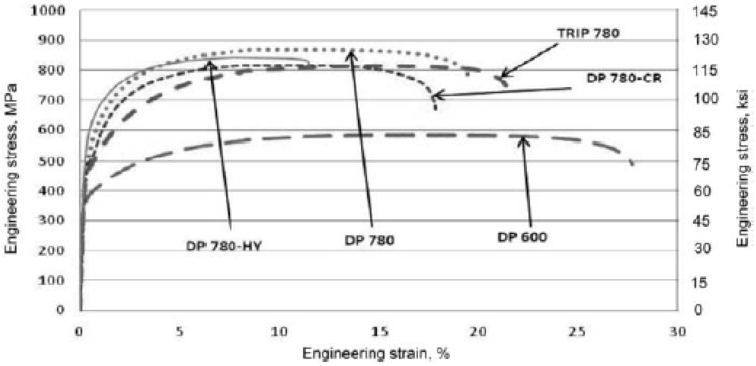

Fig 4. Engineering Stress-Strain Curve of Five Advanced High Strength Steels [8]

Studies by Grassel et al. have shown for test of TRIP and TWIP an increase of strain rate for from 1 to 800/s resulted in an increase of flow stress by 15%, but no significant difference in total elongation and strain hardening behavior [9]. There are a couple effects from higher temperature that are important to note. For most AHSS the tensile strength remains approximately the same for temperatures up to 400°C, while there is a small decrease in total elongation. Beyond 400°C the total elongation increases while the tensile strength decreases. Elevated temperatures have different effects on different AHSS [10][11].

2.2.3 Microstructure of DP Steel

DP steels microstructure is controlled with alloying elements. The effects of these elements are summarized in table 2. Figure 5 shows the continuous cooling transformation (CCT) diagram of DP steel, there is a cooling rate that needs to be controlled to obtain a desired microstructure.

Table 2. Effect of Alloying Elements in DP Steel

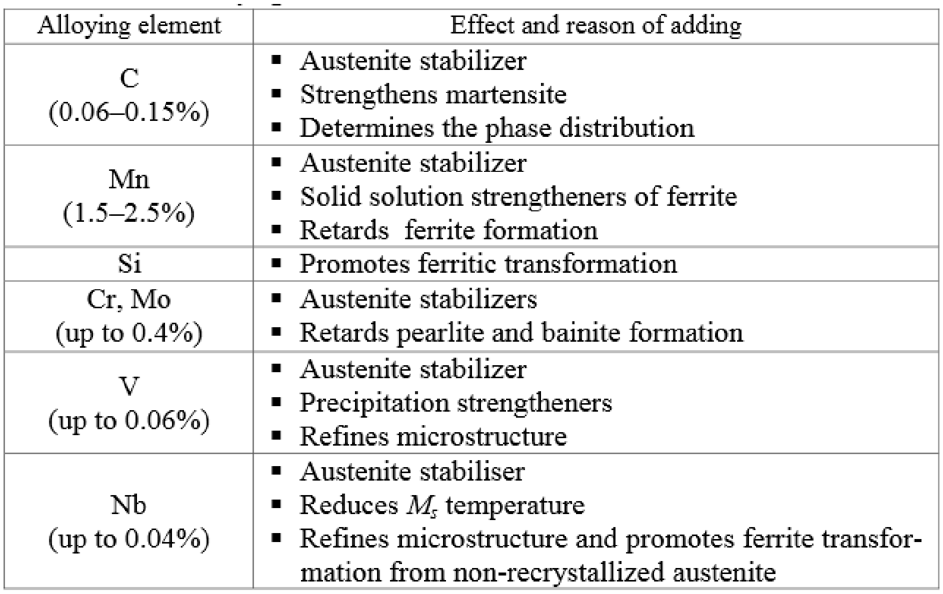

Alloying element	Effect and reason of adding
C (0.06–0.15%)	▪ Austenite stabilizer ▪ Strengthens martensite ▪ Determines the phase distribution
Mn (1.5–2.5%)	▪ Austenite stabilizer ▪ Solid solution strengtheners of ferrite ▪ Retards ferrite formation
Si	▪ Promotes ferritic transformation
Cr, Mo (up to 0.4%)	▪ Austenite stabilizers ▪ Retards pearlite and bainite formation
V (up to 0.06%)	▪ Austenite stabilizer ▪ Precipitation strengtheners ▪ Refines microstructure
Nb (up to 0.04%)	▪ Austenite stabiliser ▪ Reduces M_s temperature ▪ Refines microstructure and promotes ferrite transformation from non-recrystallized austenite

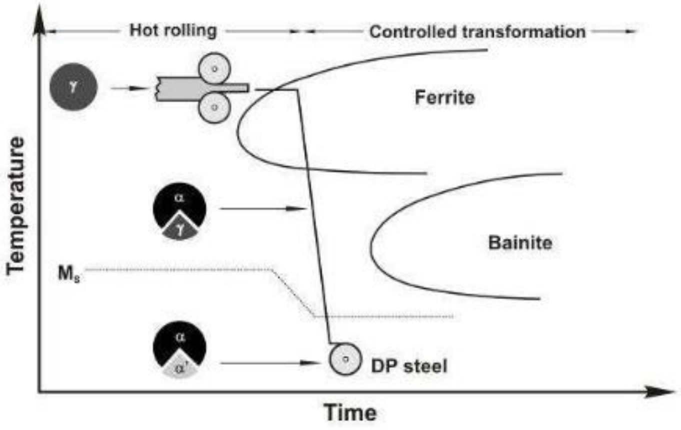

Fig 5. Cooling Schedule in the Production of DP Strips [12]

The DP steel is heated until there is a complete austenite transformation. During cooling the face centered cubic (fcc) austenite transforms into body centered cubic (bcc) ferrite, at a threshold temperature the remaining austenite transforms into body center rectangular (bcr) martensite. Martensite is essentially a pre-strained ferrite crystal, which accounts for the steels increase in strength. The cooling rate is then controlled to ensure the final microstructure consists of ferrite and martensite. However, if the steel is cooled fast enough some retained austenite remains, which can late be transformed into martensite during plastic deformation, ultimately increasing formability.

2.3 High Energy X-ray Diffraction Review

2.3.1 Background Information

X-ray diffraction is a technique capable of determining the atomic structure of a material. A crystalline or poly crystalline material is struck by a beam of x-rays, causing it to diffract into different directions. By measuring the angle of diffraction and intensity of the diffracted beam crystallographic analysis of the material can be performed to determine the composition of the microstructure.

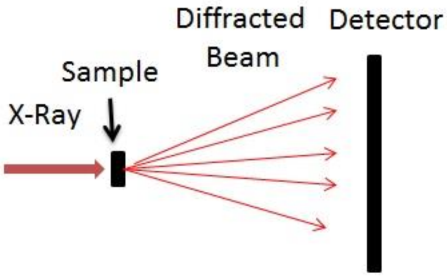

Fig 6. X-ray Diffraction Diagram

While most of the diffracted waves with cancel out in destructive interference, some waves add constructively in a few specific directions determined by Bragg's law (Equation 2.5).

$$\mathbf{2}\boldsymbol{d}\,\mathbf{sin}\,\boldsymbol{\theta} = \boldsymbol{n}\boldsymbol{\lambda} \tag{2.5}$$

Here d is the space between diffracting planes, θ is the incident angle, n is any integer, and λ is the wavelength of the beam.

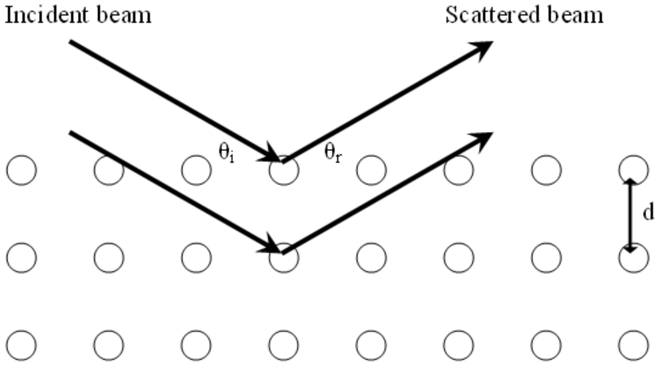

Fig 7. Bragg's Law Diagram

Constructive interference only occurs for certain *θ*'s correlating to a (*hkl*) plane. Every crystalline substance produces its own XRD pattern, which is dependent on the internal structure.

One excellent source of high-brilliance X-ray is from the Advanced Photon Source at the Argonne National Laboratory. The electrons of the X-ray are produced by a hot cathode, accelerated to 99.9999% the speed of light with an energy of 450MeV in a linear accelerator, then further accelerated to 7 GeV of energy in a booster synchrotron, finally they are injected into a storage ring and held for experimentation.

2.3.2 Advantages of High Energy X-ray Diffraction

XRD pattern is often referred to as the “Fingerprint” of a mineral or a crystalline substance, because it differs from the pattern of every other mineral or crystalline substances. Experimental patterns can be compared to known diffraction data bases to identify crystal structure. This allows observation of crystal change during the heating and cooling process, the lattice spacing can be determined and the strain in the crystal during transformation can be calculated. High sampling rate allows observation in real time of crystal transformations.

CHAPTER 3: MATERIALS AND EXPERIMENTAL DESIGN

3.1 Materials and Specimen Preparation

All the test coupons were made of ASP 1.2 mm GA DP980. The 1 ft square sheets where first cut into strips using a shear press. Next a sheer hole punch was used to add the arced sides, with a preformed strip as a guide attached to the blank strip.   The arc-sided specimen geometry is given later in figure 13.

The reasons to use this special tensile specimen geometry are: (1) to obtain the true properties of materials that have clear thermal history. In induction heating the temperature distribution over regular 2” gage length of standard tensile specimens is very difficult, and this will affect the uniformity of material property, required in standard tensile tests. The current geometry can reduce the induction heating and tensile process zone with clear thermomechanical history; (2) to improve the efficiency in specimen preparation and testing, and greatly reduce the specimen preparation time and cost.

3.2 Experimental Design

3.2.1 HEATING PROCESS CONTROL

The heat treatment process is illustrated in figure 8. There are three steps, i.e. heating, holding, and cooling. The targeted composition that is expected to improve the formability after heat treatment consists of ferrite, martensite, and austenite.

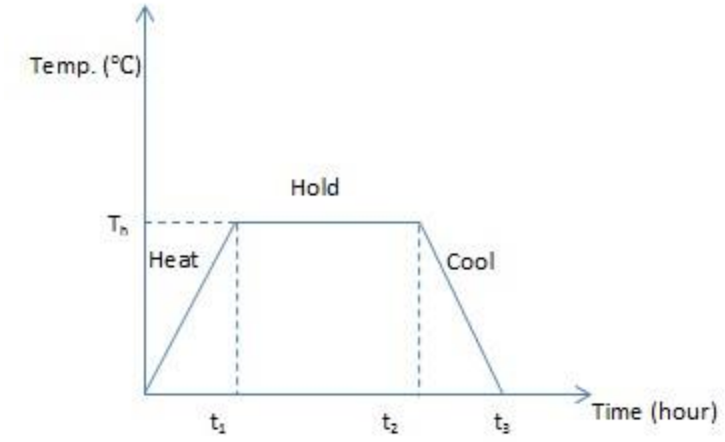

Fig 8. Heating Treatment Process

Each heating process is characterized by four parameters, e.g. the heating rate (T_h/t_1), the highest temperature T_h, the holding time (t_2-t_1) and the cooling rate ($T_h/(t_3-t_2)$). The heated test samples consisted of: 5 different highest temperatures, same holding time, and 2 different cooling rates, giving a combined 10 different heating profiles to investigate the formability after local induction heating. The other parameters such as heating rate and holding time (beyond certain transformation time) are less important for produced microstructure and were not considered here. For consistency a slow heating rate at about 100℃/min was used for all heating profiles. A 20 second holding time was enough to counteract any effects from heating rate and ensure complete microstructure transformation. After the hold period the test samples were either air cooled at a rate of about 2^{o}C/s, or water cooled at 20^{o}C/s.

The induction heating setup is illustrated in figure 9. An Omega temperature controller CN 3000 was connected to a 25 kW TOCCOtron AC in a feedback control loop. A K type thermal couple was welded to the center of the test sample and used to control the power to the induction coil, thus controlling the heating. Coupons were heated in a ferromagnetic susceptor furnace made of a stainless-steel tube, covered in a fibrous insulation ceramic, and surrounded by copper coil. A ceramic cover was used to hold the coupon in place and minimize thermal variation (figure 10).

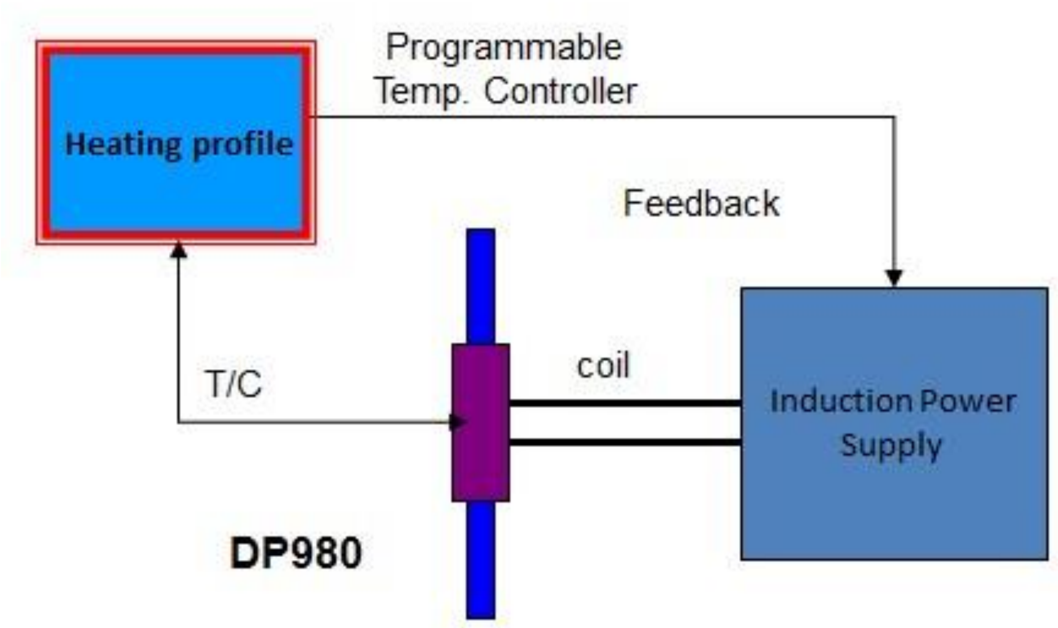

Fig 9. Heating Equipment Setup

Fig 10. Induction Furnace

3.3 Heating Parameters Selection and Temperature Data Acquisition

The temperatures selected are listed in table 3, from 800℃ to 1000℃ with corresponding temperature controller setup. The entire heating process was also recorded by an Omega 8-Channel Thermocouple/Voltage Input USB Data Acquisition Module.

Table 3. Highest Temperatures Selection and Corresponding Controller Setup

Highest Temp.	P(PR Band)	I(Reset)	D(Rate)
800	100	0.30	0
850	100	0.30	0
900	95	0.35	0
950	95	0.35	0
1000	90	0.40	0

The heating profile for each coupon is shown in figure 11 and 12. Both graphs show a consistent heating profile. There were minor differences between the heating rate, and all samples received the same hold time. The cooling rate for each coupon was about the same, ensuring a consistent end product. The temperature gradient in and out of the furnace were also measured. These measurements showed a significant difference in temperature over a small distance. The temperature can drop 300 degrees in a few millimeters after leaving the furnace. This means accurate reading can only be taken in few locations.

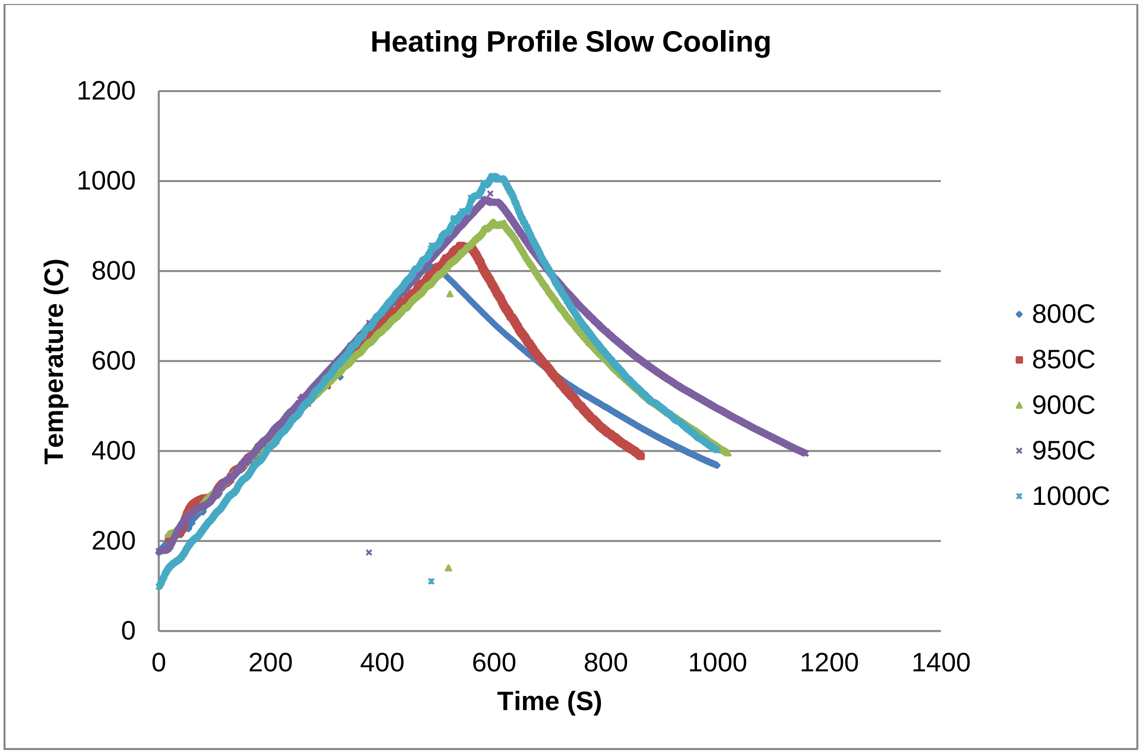

Fig 11. Slow Cooling Rate

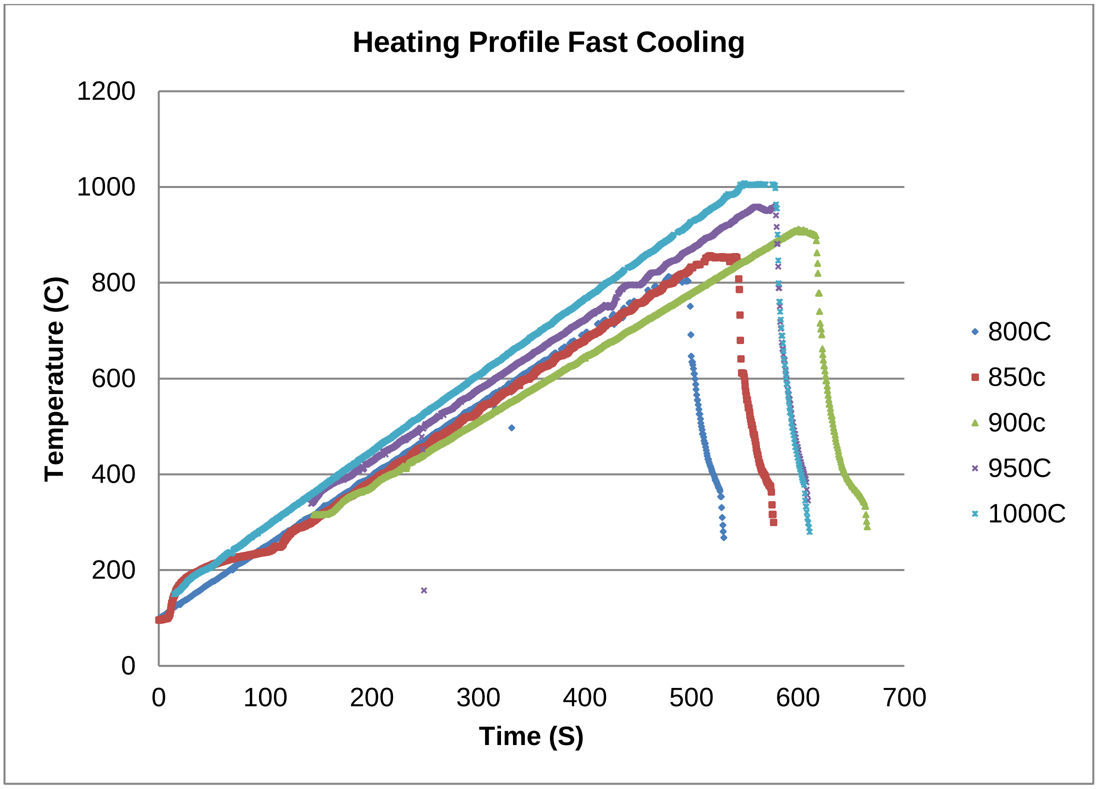

Fig 12. Fast Cooling Rate

3.4 Hardness Test

A Wilson Tukon 2100 Instron hardness testing machine was used to first verify the effects of the induction heating. A Vickers hardness indenter set at1 kg force with a 10 second impress time was used for each test sample and a piece of the original material as a control. Each sample was placed on a small piece of clay and pressed with a cylindrical punch to level, then tested 5 times in the location of the main controlling thermal couple. Image measurement software was then used to measure the diagonals of the indentation, which was then converted to Vicker's hardness using equation 3.1.

$$NHV = \frac{1.854P}{L^2} \tag{3.1}$$

Where *P* is the force in kg and *L* is the length of the diagonals of the depression made in mm. The initial test were performed without altering the surface of the coupon. This was found to give high variation to the results, due to coarse wave pattern from the outer coating. The data was retaken using lightly sanded pieces to remove the coating, the result of which was more accurate reading of hardness but no significant difference in the overall hardness.

3.5 Microstructure Observations

Optical microscopy was used for microstructure observations. Samples were cut from the tensile strip near the weld location of the thermal couple. They were then prepared using sanding polishing and grinding. The samples were then etched with a solution of 2% nital, for 10 to 20 seconds. The etched samples were then examined under an Olympus metallurgical microscope, with an attached OptixCam Summit 9MP camera attached.

3.6 Tensile Test

A tensile test with an arc coupon (figure 13) was used to measure elongation and the r value. The advantage of those test over convention test with a gauge length is the measurement can be focused on a location where the heat profile is known.

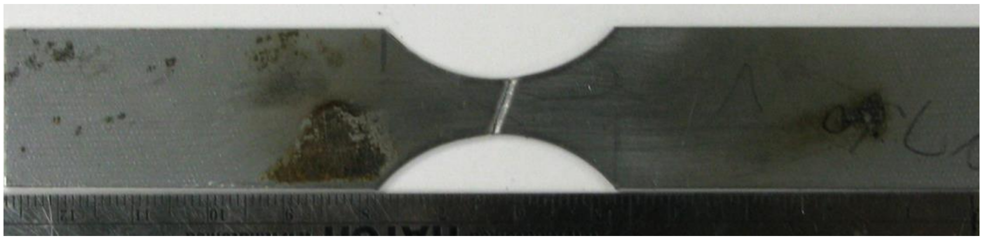

Fig 13. Arc Side Tensile Coupon

The heated and un-heated test strips were tested using an Instron 8801 Tensile Testing Machine controlled with an Instron controller 8800 and a ±100 kN axial force capacity. The samples were mounted using hydraulic grips with a hydraulic pressure of 2000psi. The controller was set to load control mode during loading to ensure no tension or compression before the start of the test.

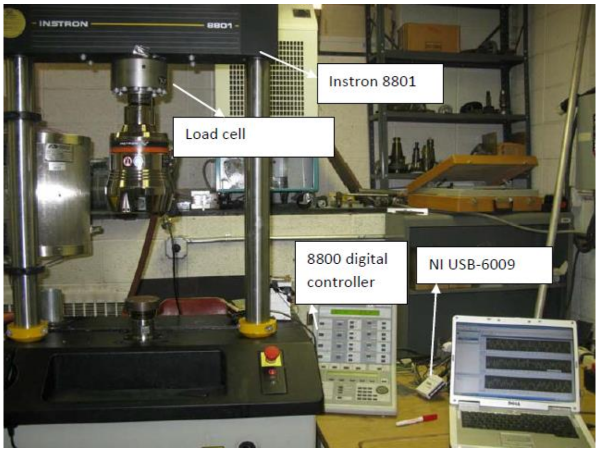

Fig 14. Instron Test Set Up

Each strip was tested at a constant increase in position. A NI USB-6009 was used with LabView SignalExpress to record the force and displacement output voltage signals. These signals were then converted to scientific units using MatLab. The first set of tests used a camera to measure the change in the width this was then used to calculate the elongation strain vs. stress. The next set of tests where stopped intermittently and a micrometer was used to measure the dimensions of the width (w) and thickness (t). These measurements were then used to calculate the width strain (ε_w) and the thickness strain (ε_t) (Equation 3.2 & 3.3).

$$\boldsymbol{\varepsilon_w = ln\left(\frac{w}{w_o}\right)} \tag{3.2}$$

$$\boldsymbol{\varepsilon_t = ln\left(\frac{t}{t_o}\right)} \tag{3.3}$$

These values were then used to calculate the strain elongation (Equation 3.4). The true stress (Equation 3.5) was finally calculated using the measured w, t, and the force (F) during each intermission.

$$\boldsymbol{\varepsilon_l = \varepsilon_w + \varepsilon_t} \tag{3.4}$$

$$\boldsymbol{\sigma_l = \frac{F}{(w*t)}} \tag{3.5}$$

3.7 X-ray Diffraction Analysis

In-situ X-ray diffraction from a synchrotron source was conducted on DP980. A sample was prepared by cutting a 1 mm square from an unheated test strip. The sample was heated and cooled at a controlled rate by a furnace with water cooling. The furnace was installed in the beam line a distance of 1600cm from the digital detector and a beam size of 0.10804Å was used. The heating rate was 50 ^{o}C/min, and cooling rate was 60 ^{o}C/min. During testing the diffracted angles and intensities were recorded in a Tiff image file, at a frequency of 10 Hz. Three trials of DP980 were conducted each with the same heating and cooling rate, but with different hold times.

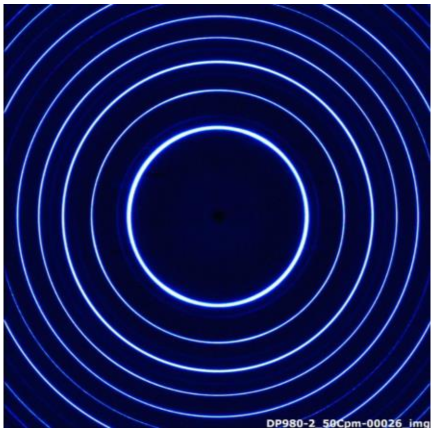

Fig 15. Example Bragg's Diffraction Ring

The raw diffraction data of the three trials was converted to Braggs diffraction rings (figure 15) images using FIT2D analysis software. A calibrated sample was measured and used to calibrate the software. The diffraction rings were then integrated to produce the 2θ vs. intensity graph. The series of graphs where combined into a movie and used to identify key events. Once important frames were identified Match! 2 software package was used to identify the phases of the experimental, data with the known diffraction patterns of the Crystallography open database (COD), and International Center for Diffraction Data (ICDD).

CHAPTER 4: RESULTS AND DISCUSSION

4.1 Microhardness Results

The results of the hardness test (Figure 16) were first used to identify if any change had occurred. Below 800°C there is little change in hardness within the error range, this steel is also known to bake harden below 400°C. The slow cooling rate produced a lower hardness, this is attributed to less retained austenite.

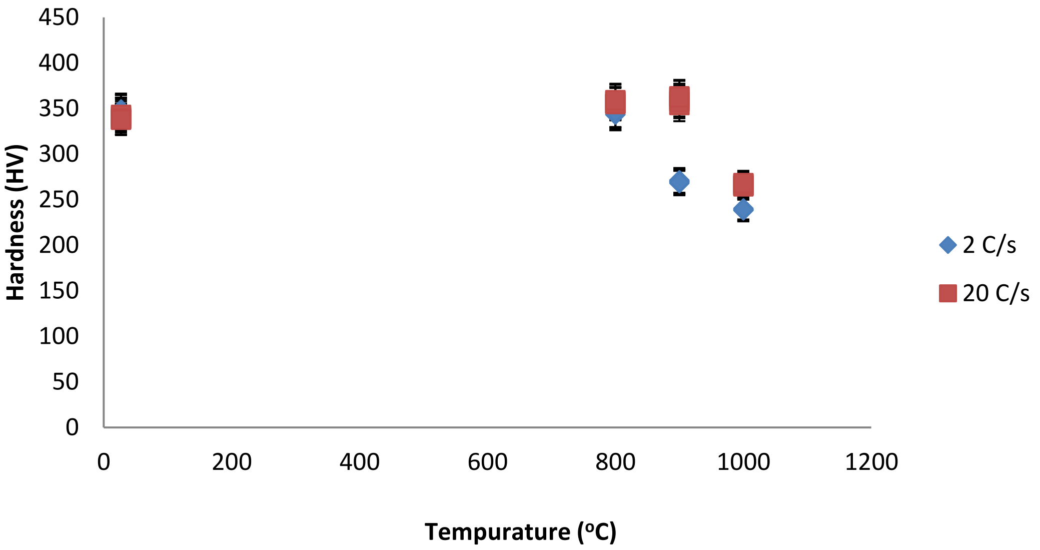

Fig 16. Hardness Test Results for Slow and Fast Cooling Rates

4.2 Tensile Test Results

The results of the initial tensile test are displayed in figures 17 and 18. These graphs show a significant increase in the elongation above the original sample with no heating. The result however vary on which heating profile shows the highest increase in elongation with the best result in the range of 800 - 900°C. The tests at 1000°C show the greatest variation in max elongation.

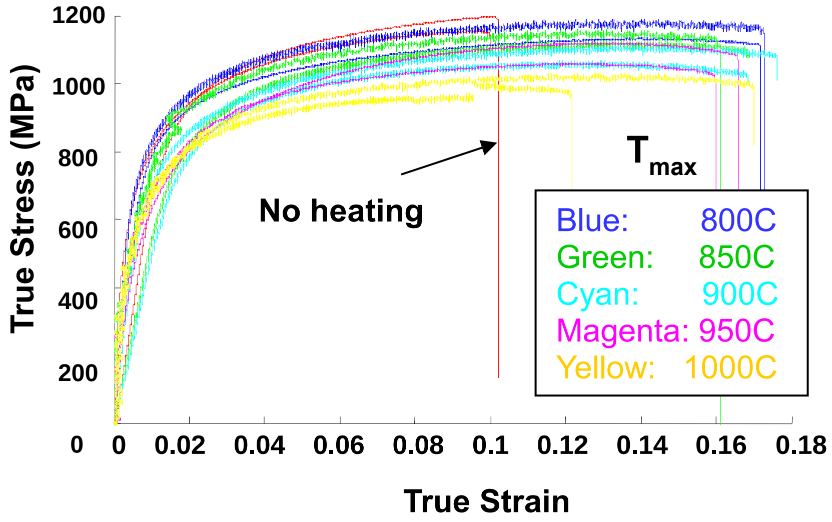

Fig 17. Elongation vs. True Strain for Slow Cooling

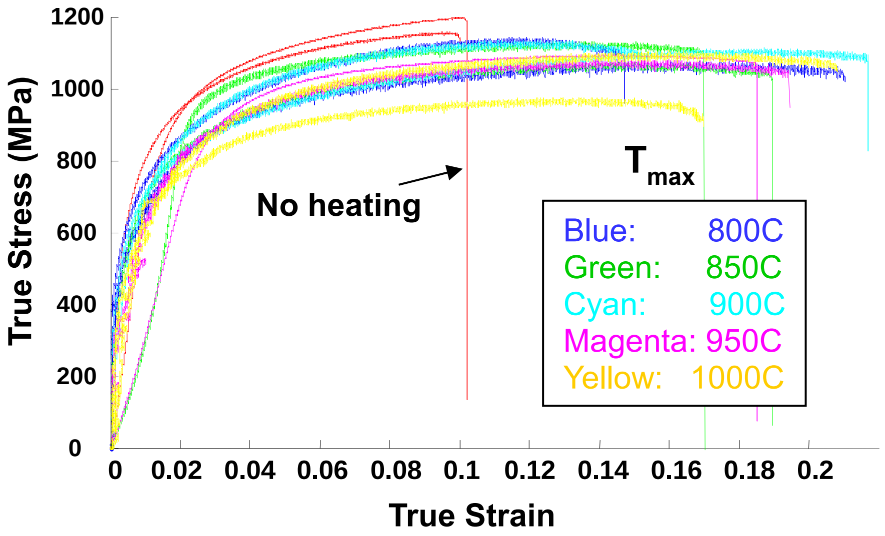

Fig 18. Elongation vs. True Strain for Fast Cooling

Figure 19 compares the results of the UTS against various max temperatures and cooling rates. It shows there is a general decrease in the UTS for all trials, the greater the temperature the greater the reduction in UTS. The test strips that were fast cooled show a general trend towards lower UTS. The low UTS was with in the acceptable range and means an increase in formability.

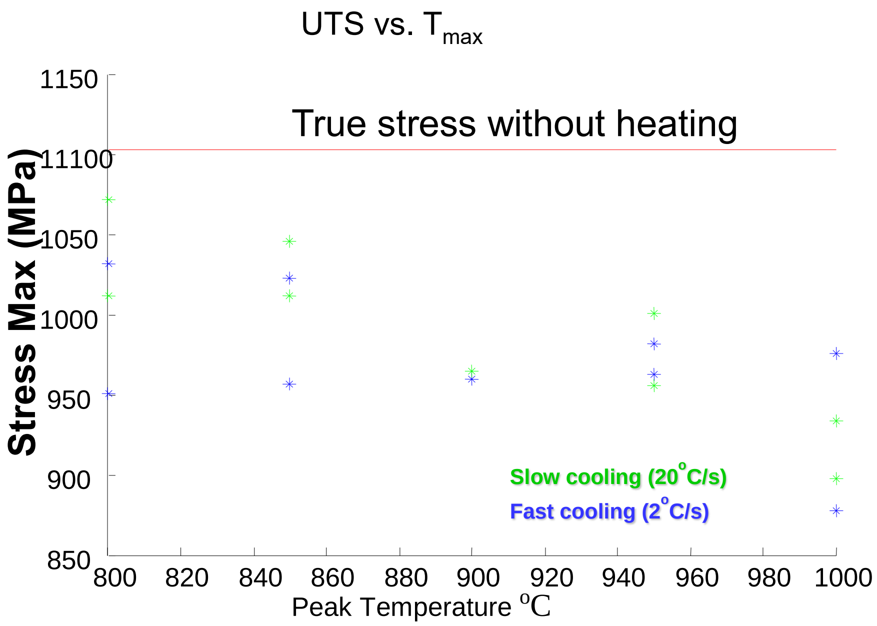

Fig 19. UTS Vs. Maximum Temperature

The elongation versus the maximum temperature is shown in figure 20. Fast cooled test strip shows a higher amount of elongation than trails at a similar temperature. This result helps confirm the assumption of more retained austenite from fast cooling from the hardness test. Austenite is both a harder material than ferrite and transforms to martensite during plastic strain, increasing overall formability. All tests showed improved elongation over the as received test.

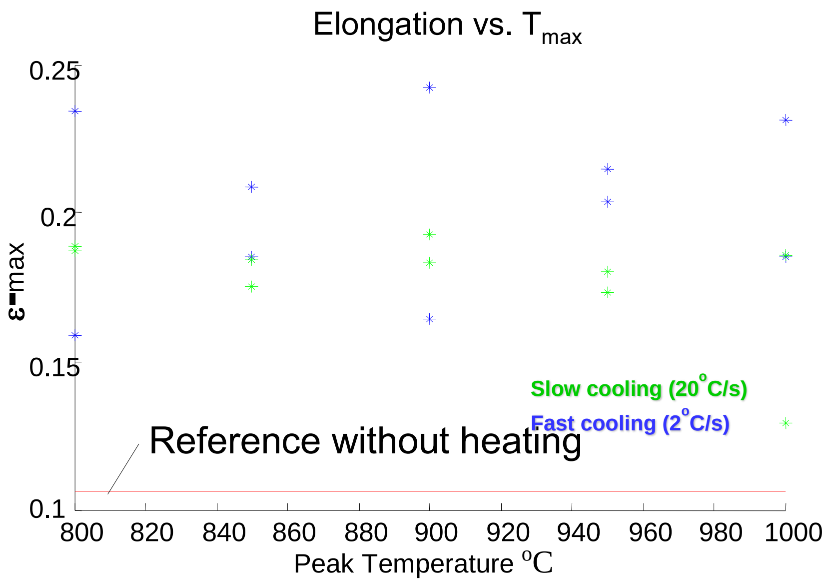

Fig 20. Elongation vs. T Max

It is interesting to see the evolution of R value during tensile deformation, where R is the ratio of the thickness strain to the width strain, $\varepsilon_t/\varepsilon_w$. The results of measurements for the R value are shown in Figure 21. At lower longitudinal strain the R value is at the magnitude of 1, similar to common R value range that does not have strong texture. However, past a strain of 0.1 the R value decreases. The greater the maximum temperature the greater the increase in longitudinal strain, while the R value reaches the minimum value that can be as low as 0.4, probably related to the second principal stress development in the width direction from the current specimen geometry with two arced sides, which promoted the width deformation and reduced the thickness deformation, and this stress-state effect initiated from the two width edge, and with the increase in the longitudinal strain this effect gradually penetrated into the entire width.

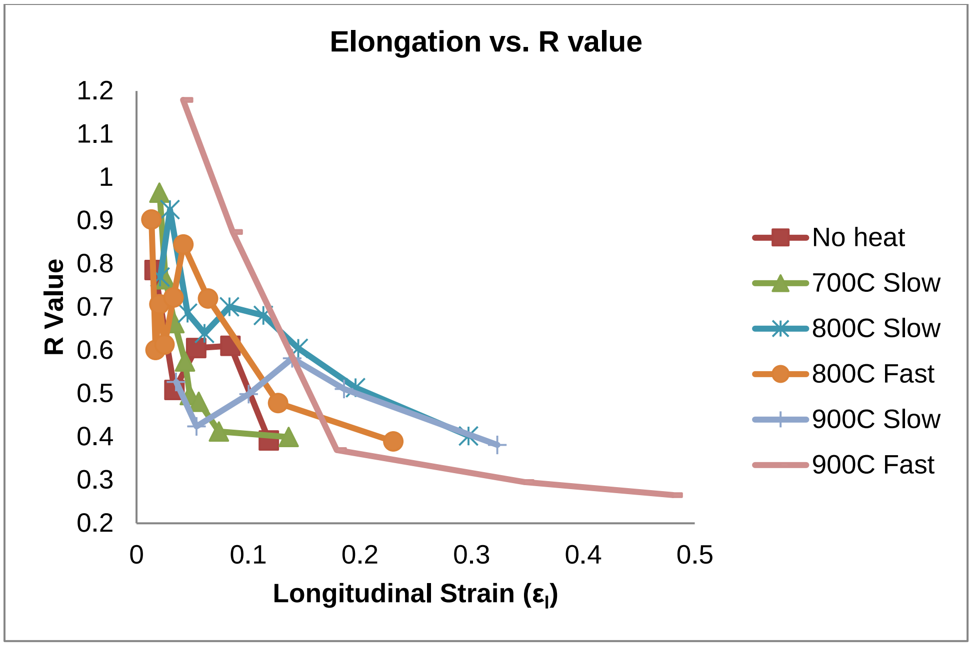

Fig 21. Elongation vs. R Value

4.3 Microstructure

Images of the microstructure were taken on each of the heated sample (Figures 21, 22, 23, 24). The larger martensite clusters have been dissolved via heating. The different cooling rates show vastly different microstructures. The coupons that were cooled quickly have finer grain structure and show more ferrite than their slow cooled counterpart. Samples heated to 800°C have a finer structure than samples heated to 1000°C. A finer grain structure is associated with increase in hardness, yield strength, tensile strength, fatigue strength and impact strength. The gain size is so fine it is difficult to separate ferrite from austenite, or accurately measure the volume fraction of martensite with optical microcopy.

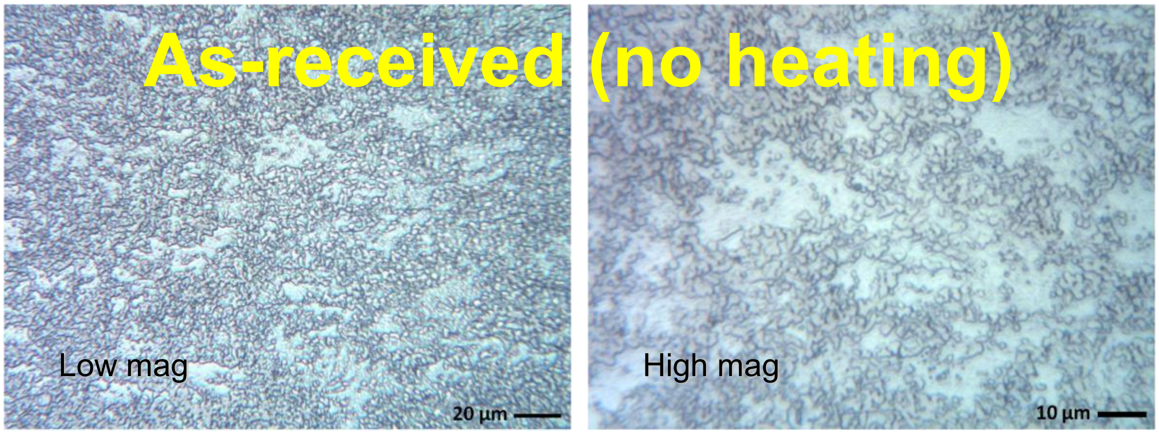

Fig 22. Microstructure No Heating

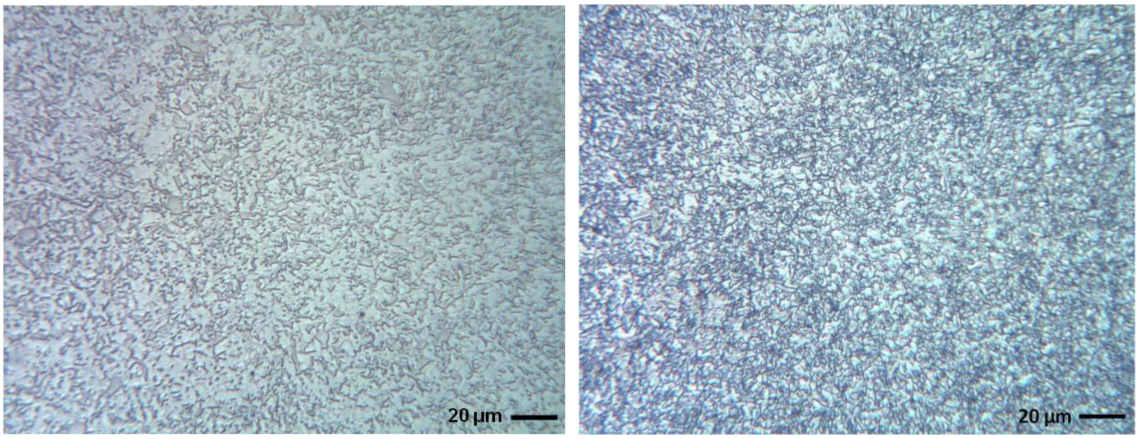

Fig 23. Microstructure 800 C Slow & Fast Cooling

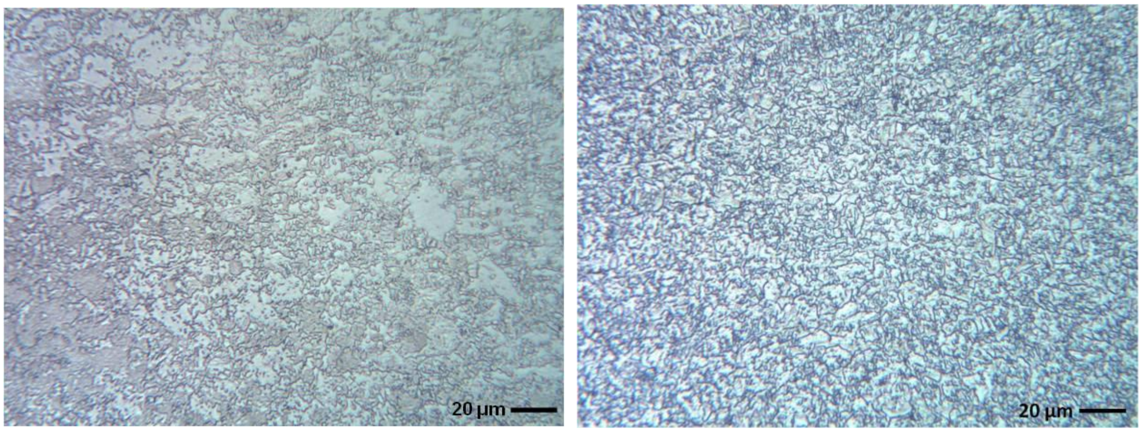

Fig 24. Microstructure 900 C Slow & Fast Cooling

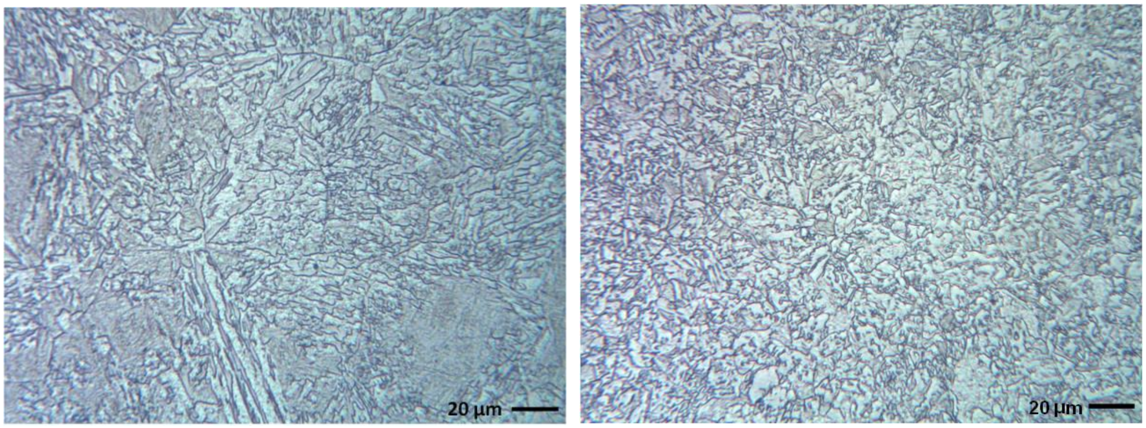

Fig 25. Microstructure 1000 C Slow & Fast Cooling

4.4 X-ray Diffraction Results

The as received DP980 diffraction pattern is shown in figure 26. The first peak is the [101] plane normal of ferrite steel, this is followed by the [200], [211], and [202]. However, part of the peak is integrated with a martensite peak, this is because the geometry and size of ferrite and martensite are similar. Figure 27 shows the diffraction pattern during heating, which shows the disappearance of the [101] ferrite peak and the appearance of the [111] austenite peak. The phase change was tracked by a video to identify at which temperature the change began, at what rate did the change occur, and what the final end product were.

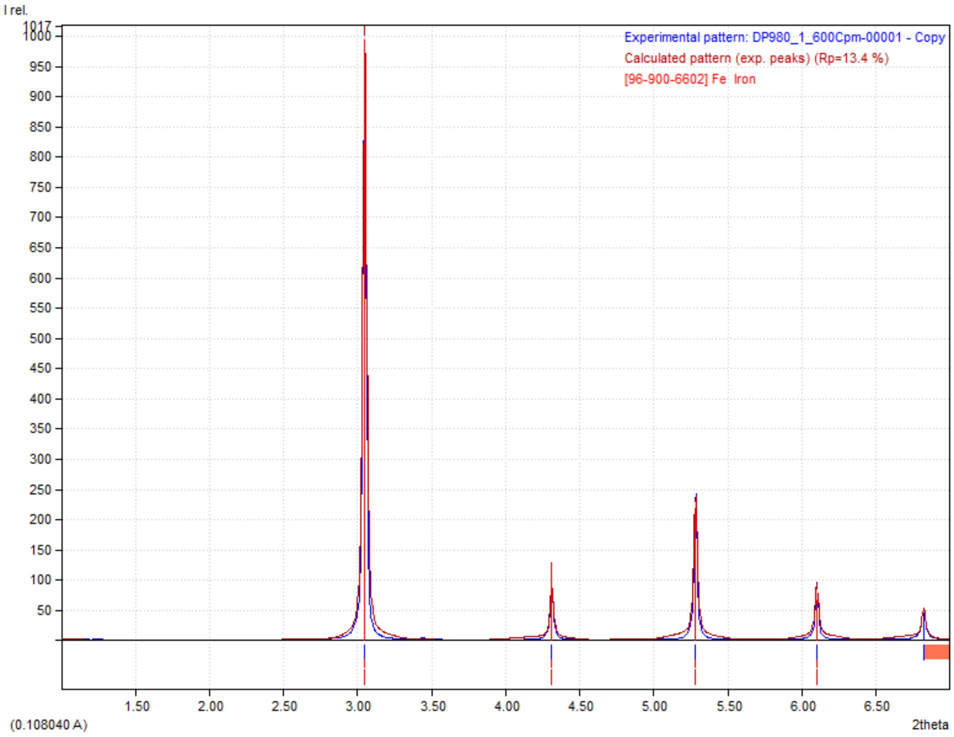

Fig 26. Integrated 2 Theta vs Intensity Graph

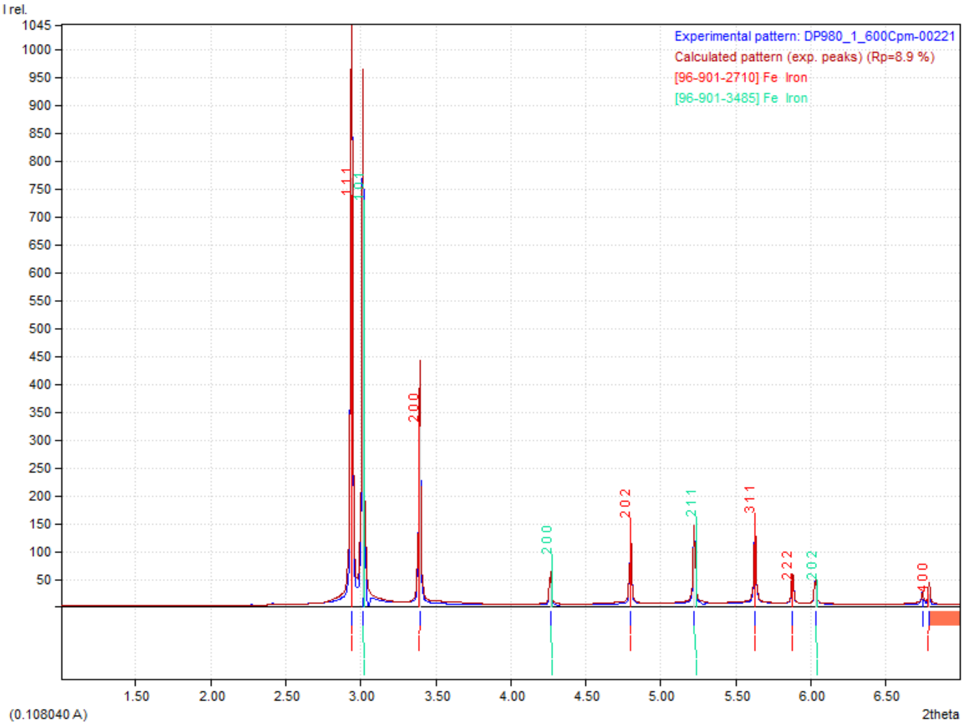

Fig 27. Integrated 2 Theta vs Intensity Graph

The results of the final phase fractions are shown in table 4. With a 60°C/s cooling rate there is about 10% retained austenite, compared to the initial concentration of 0%. This increase helps account for increase in formability seen in the tensile test results.

Table 4. Final Phase Volume of In-Situ Trials

Hold time (s)	**Ferrite %**	**Austenite%**
600	89.3	10.7
100	87.2	12.8
50	92.7	7.3

The purpose of the in-situ testing is to identify the exact reheating parameters that can be applied for industrial applications. Figure 28 shows a comparison of different trials with same parameters except different hold times. It can be clearly seen that in heating a complete phase transformation does not always occur at the same temperature. The first column shows a trial held for 50 seconds at the highest temperature, the transformation of ferrite to austenite began at around 800°C and was complete by the time the sample reached 950°C. The second column shows a trial with a hold time of 100 seconds, this time transformation from ferrite to austenite began late and did not complete at 950°C. A third trial with a hold time of 600 seconds showed nearly identical results to the 50 second trial. One possible explanation for this occurrence is the metal was not completely mixed. After cooling the final phase volume of each sample seems similar for these two samples with different holding time at the maximum temperature, with the peak of retained austenite clearly seen. The minor difference in phase fraction and the produced microstructure (e.g. grain size) associated with the holding time may have significant effect on the mechanical properties. More specifically, the retained austenite phase can contribute to the enhanced formability through a strain-induced austenite to martensite phase transformation. It is known that DP and TRIP steels have the same or similar alloy chemistry and their microstructures only differ by heat treatment, and TRIP steel has a higher formability than DP of similar strengths.

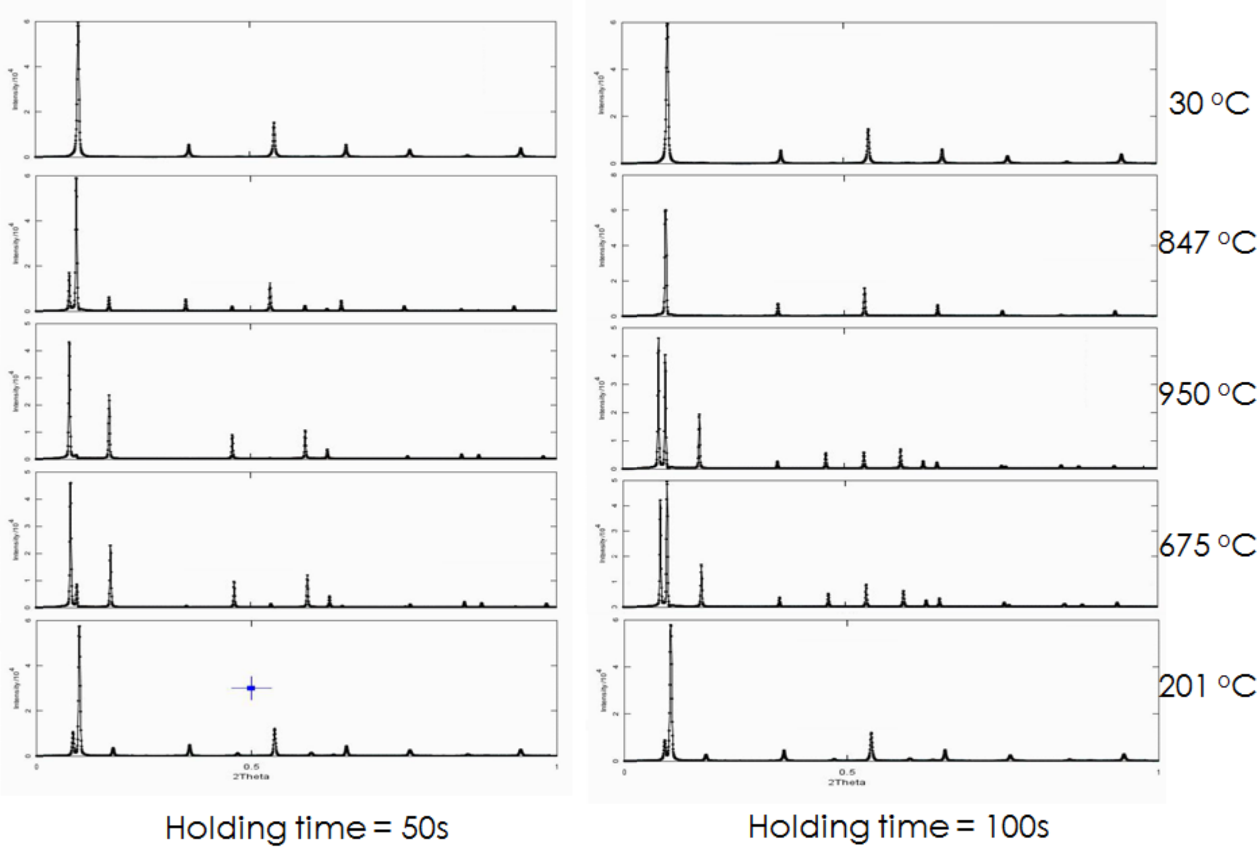

Fig 28. Comparison of 2 Theta Graphs for Same Heating and Cooling Rate with Different Hold Time

Speed of manufacturing is a main concern for the automotive production. Therefore, it is necessary to heat the metal as fast as possible to ensure a complete phase change, this will allow the time to be used for the final phase fraction volume to be controlled by the cooling rate. It is also shown that air cooling is about the correct rate to produce a microstructure with retained austenite, ultimately increasing the formability.

CHAPTER 5: CONCLUSION

This experiment demonstrates it is possible to increase the formability of DP steel. The increase in formability is attributed to a finer grain structure and increase in retained austenite.

It was found peak heating temperature and cooling rate are the two most important parameters. The results were first verified using hardness tests, which showed a reduction in hardness above 800^{o}C, with the fast cooled trial being harder. Within the range of 800 -1000^{o}C, and with a cooling rate of 2-20^{o}C results showed reduced strength and increased fracture strain relative to the as-received DP980. The ideal result for manufacturability is dependent on the application of the sheet steel. The new local tensile property evaluation technique was developed (with arced test strip). Microstructure observation indicates that; cooling rate affects reduction of martensite volume, which affect both strength and formability. In-situ x-ray diffraction was used to identify key temperatures when transformation occurs and final phase volume in real time. X-ray diffraction conformed an austenite initiation temperature around 850^{o}C and a rapid full transformation to full austenite by 950^{o}C. The in-situ also showed full transformation did not always occur, although the end product was similar when compared to a trail with full transformation. This observation would not have been possible without the observations of microstructure change during heating and cooling in-situ.

CHAPTER 6: FUTURE WORK

Further x-ray diffraction testing should be done with varying cooling rates. By testing cooling rates between 2 – 100^{o}C/s. A function can be developed between cooling rate and retained austenite. Next the gauge area of water jet cut tensile strip should be heat treated with the same cooling rates as the x-ray tests. Finally, tensile tests should be performed on the treated strips, to develop a function that can be used to predict material strength from cooling rate.

Micro hardness test and optical microscopy tests should be performed on the next test samples. The results should be compared to the previous trials. Scanning electron microscopy (SEM) can finally be used to verify the final phase fractions determined by the x-ray diffraction. It should be noted that studies have shown inconstancy between volume fraction determined by different methods, these studies have shown neutron and x-ray diffraction of the most accurate of the methods.

APPENDIX - ELONGATION TABLE

Table 5. Elongation Data

Coupon	Highest Temp.	Cooling Tate	Elongation
1	800	Fast	0.2341
2	800	Fast	0.1588
3	800	Slow	0.1866
4	800	Slow	0.1988
5	850	Fast	0.2098
6	850	Fast	0.1854
7	850	Slow	0.1750
8	850	Slow	0.1840
9	900	Fast	0.2423
10	900	Fast	0.1641
11	900	Slow	0.1925
12	900	Slow	0.1833
13	950	Fast	
14	950	Fast	0.2146
15	950	Slow	
16	950	Slow	
17	1000	Fast	0.2314
18	1000	Fast	0.1853
19	1000	Slow	0.1856
20	1000	Slow	0.1291

REFERENCES

[1] S. Kalpakjian and S. R. Schmid, *Manufacturing processes for engineering materials*. Pearson education, 2010.

[2] W. F. Hosford and R. M. Caddell, *Metal forming: mechanics and metallurgy*. Cambridge University Press, 2011.

[3] D. Bhattacharya, “Developments in advanced high strength steels,” in *The Joint International Conference of HSLA Steels*, 2005, pp. 70–73.

[4] J. R. Shaw and B. K. Zuidema, “2001-01-3041 New High Strength Steels Help Automakers Reach Future Goals for Safety, Affordability, Fuel Efficiency and Environmental Responsibility,” *SAE TRANSACTIONS*, vol. 110, no. 5, pp. 976–983, 2001.

[5] E. G. Opbroek, *Advanced High Strength Steel (AHSS) Application Guidelines*. Version, 2005.

[6] J. Shaw, M. CHEN, and K. WATANABE, “Metal forming characterization and simulation of advanced high strength steels,” *SAE transactions*, vol. 110, no. 5, pp. 926–935, 2001.

[7] X. Chen, M. Shi, G. Chen, and M. Kamura, “Crash performances of advanced high strength steels of DP780, TRIP780 and DP980,” *Metallurgy*, vol. 2013, pp. 10–10, 2005.

[8] A. Nasser, A. Yadav, P. Pathak, and T. Altan, “Determination of the flow stress of five AHSS sheet materials (DP 600, DP 780, DP 780-CR, DP 780-HY and TRIP 780) using the uniaxial tensile and the biaxial Viscous Pressure Bulge (VPB) tests,” *Journal of Materials Processing Technology*, vol. 210, no. 3, pp. 429–436, Feb. 2010.

[9] O. Grässel, L. Krüger, G. Frommeyer, and L. . Meyer, “High strength Fe–Mn–(Al, Si) TRIP/TWIP steels development — properties — application,” *International Journal of Plasticity*, vol. 16, no. 10–11, pp. 1391–1409, 2000.

[10] K. Mori, S. Maki, and Y. Tanaka, “Warm and Hot Stamping of Ultra High Tensile Strength Steel Sheets Using Resistance Heating,” *CIRP Annals - Manufacturing Technology*, vol. 54, no. 1, pp. 209–212, 2005.

[11] M. . Berrahmoune, S. Berveiller, K. Inal, A. Moulin, and E. Patoor, “Analysis of the martensitic transformation at various scales in TRIP steel,” *Materials Science and Engineering: A*, vol. 378, no. 1–2, pp. 304–307, Jul. 2004.

[12] R. KUZIAK, R. KAWALLA, and S. WAENGLER, “Advanced high strength steels for automotive industry,” *Archives of Civil and Mechanical Engineering*, vol. 8, no. 2, pp. 103–117, 2008.

ABSTRACT

INDUCTION LOCAL SOFTENING OF ADVANCED HIGH STRENGTH STEELS

by

JORGE CISNEROS

December 2018

Advisor: Xin Wu

Major: Mechanical Engineering

Degree: Master of Science

This study was to determine the important parameters regarding induction local softening of dual phase steel with improved manufacturability for autobody stamping. Samples were inductively heat-treated, and then tested using micro hardness test, tensile test, microstructure analysis, and x-ray diffraction analysis. It was found that above 800ºC there was a significant reduction in hardness. The cooling rate was found to be the most important parameter affecting the final properties of the steel. The tensile test showed a significant increase in total elongation with a small reduction in ultimate tensile strength. These factors led to the ultimate increase in formability. X-ray diffraction was used to show the connection between retained austenite and the enhanced formability.

AUTOBIOGRAPHICAL STATEMENT

My interest in engineering dates to preschool where I dreamed of designing the latest space ships. Throughout elementary school science was always my favorite subject and I spent most of my time building and designing as a child.

During my undergraduate career at the University of Michigan, I enjoyed the full range of fundamental engineering classes. This helped to solidify my love of the engineering and design process. Upon graduating I took a position as a design engineer with a tool company in Indiana. There I designed work holding devises such as, chucks, face drivers, and steady rests. In order to create long life products unique material and processes are used. It was here that I gained valuable knowledge of material consideration concerned with design.

After gaining some valuable real world experience I began my graduate studies in Mechanical Engineering at Wayne State University in Detroit, MI. It was there I met my advisor Dr. Xin Wu who inspired me to experiment with advanced high-strength steels. He taught me to push the limits of test capabilities by building custom apparatuses for experiments. He also introduced me to high energy X-ray diffraction at the national labs, which allowed me to complete my research. This then led to a valuable internship opportunity at the Oakridge National Lab, which allowed me to vastly expand my knowledge of X-ray diffraction. With these advanced techniques I continue my research in nano-materials for fabrications of advanced high strength steels.